Hydrous upwelling across the mantle transition zone beneath the Afar Triple Junction

AGU PUBLICATIONS

Geochemistry, Geophysics, Geosystems

RESEARCH ARTICLE

10.1002/2014GC005648

Hydrous upwelling across the mantle transition zone beneath the Afar Triple Junction

D. A. Thompson[1,2,3], J. O. S. Hammond[4], J.-M. Kendall[3], G. W. Stuart[2], G. R. Helffrich[3,5], D. Keir[6], A. Ayele[7], and B. Goitom[3,8]

[1]School of Geosciences, University of Aberdeen, Aberdeen, UK, [2]School of Earth and Environment, Institute of Geophysics and Tectonics, University of Leeds, Leeds, UK, [3]School of Earth Sciences, University of Bristol, Bristol, UK, [4]Department of Earth Science and Engineering, Imperial College London, London, UK, [5]Earth-Life Science Institute, Tokyo Institute of Technology, Tokyo, Japan, [6]National Oceanography Centre Southampton, University of Southampton, Southampton, UK, [7]Institute of Geophysics, Space Science and Astronomy, Addis Ababa University, Addis Ababa, Ethiopia, [8]Department of Earth Science, Eritrea Institute of Technology, Asmara, Eritrea

Key Points:
- Evidence for ongoing upwelling from the deep mantle beneath East Africa
- Uniform transition zone thickness suggests weak thermal anomaly (<100 K)
- Upwelling is hydrous and likely driven in part by compositional buoyancy

Supporting Information:
- Supporting Information

Correspondence to:
D. A. Thompson,
david.thompson@abdn.ac.uk

Citation:
Thompson, D. A., J. O. S. Hammond, J.-M. Kendall, G. W. Stuart, G. R. Helffrich, D. Keir, A. Ayele, and B. Goitom (2015), Hydrous upwelling across the mantle transition zone beneath the Afar Triple Junction, *Geochem. Geophys. Geosyst.*, *16*, 834–846, doi:10.1002/2014GC005648.

Received 10 NOV 2014
Accepted 20 FEB 2015
Accepted article online 26 FEB 2015
Published online 24 MAR 2015

Abstract The mechanisms that drive the upwelling of chemical heterogeneity from the lower to upper mantle (e.g., thermal versus compositional buoyancy) are key to our understanding of whole mantle convective processes. We address these issues through a receiver function study on new seismic data from recent deployments located on the Afar Triple Junction, a location associated with deep mantle upwelling. The detailed images of upper mantle and mantle transition zone structure illuminate features that give insights into the nature of upwelling from the deep Earth. A seismic low-velocity layer directly above the mantle transition zone, interpreted as a stable melt layer, along with a prominent 520 km discontinuity suggest the presence of a hydrous upwelling. A relatively uniform transition zone thickness across the region suggests a weak thermal anomaly (<100 K) may be present and that upwelling must be at least partly driven by compositional buoyancy. The results suggest that the lower mantle is a source of volatile rich, chemically distinct upwellings that influence the structure of the upper mantle, and potentially the chemistry of surface lavas.

1. Introduction

The upwelling of material from the lower mantle to the base of the lithosphere is hypothesized as being a primary planetary geodynamic process [*Morgan*, 1971], and it is widely believed that the driving force behind these upwellings is thermal convection initiated due to heating at the core-mantle boundary [*Beier et al.*, 2008]. However, it is unlikely that convection in the Earth is purely isochemical [*Stixrude and Lithgow-Bertelloni*, 2012], and heterogeneous mantle composition may also lead to variations in density and hence buoyancy. Despite this expectation, the extent to which upwellings and their associated surface volcanism are driven by temperature or compositional variations in the mantle is currently poorly constrained by observations [*Ito and van Keken*, 2007]. The mineralogical phase changes that produce the 410, 520, and 660 km seismic discontinuities (olivine → wadsleyite, wadsleyite → ringwoodite, and ringwoodite → perovskite + magnesiowüstite, respectively, and herein referred to as the *410*, *520*, and *660*) are sensitive to both temperature and composition [*Helffrich*, 2000], equipping the mantle transition zone (MTZ) with mechanisms to test upwelling hypotheses. Due to the opposite signs of the Clapeyron slopes associated with the *410* and the *660*, regions of warmer than average mantle, a likely situation if upwelling is driven by thermal buoyancy, should produce a thinner than expected MTZ. This has been observed in certain localities (e.g., ~20 km beneath Iceland suggesting an excess temperature of 150 K) [*Shen et al.*, 1998], but other global observations have suggested that there is little correlation of a thinner MTZ thickness with the location of mantle upwellings [*Tauzin et al.*, 2008].

In this study, we analyze new seismic data from recent deployments located on the Afar Triple Junction (Figure 1), the youngest flood basalt province in the world and where the geochemistry of recent volcanism strongly suggests a lower-mantle source [*Pik et al.*, 2006]. The region is characterized by widespread ~30 Ma volcanism, initiation of continental rifting ~29 Ma and continued yet less voluminous volcanism to the

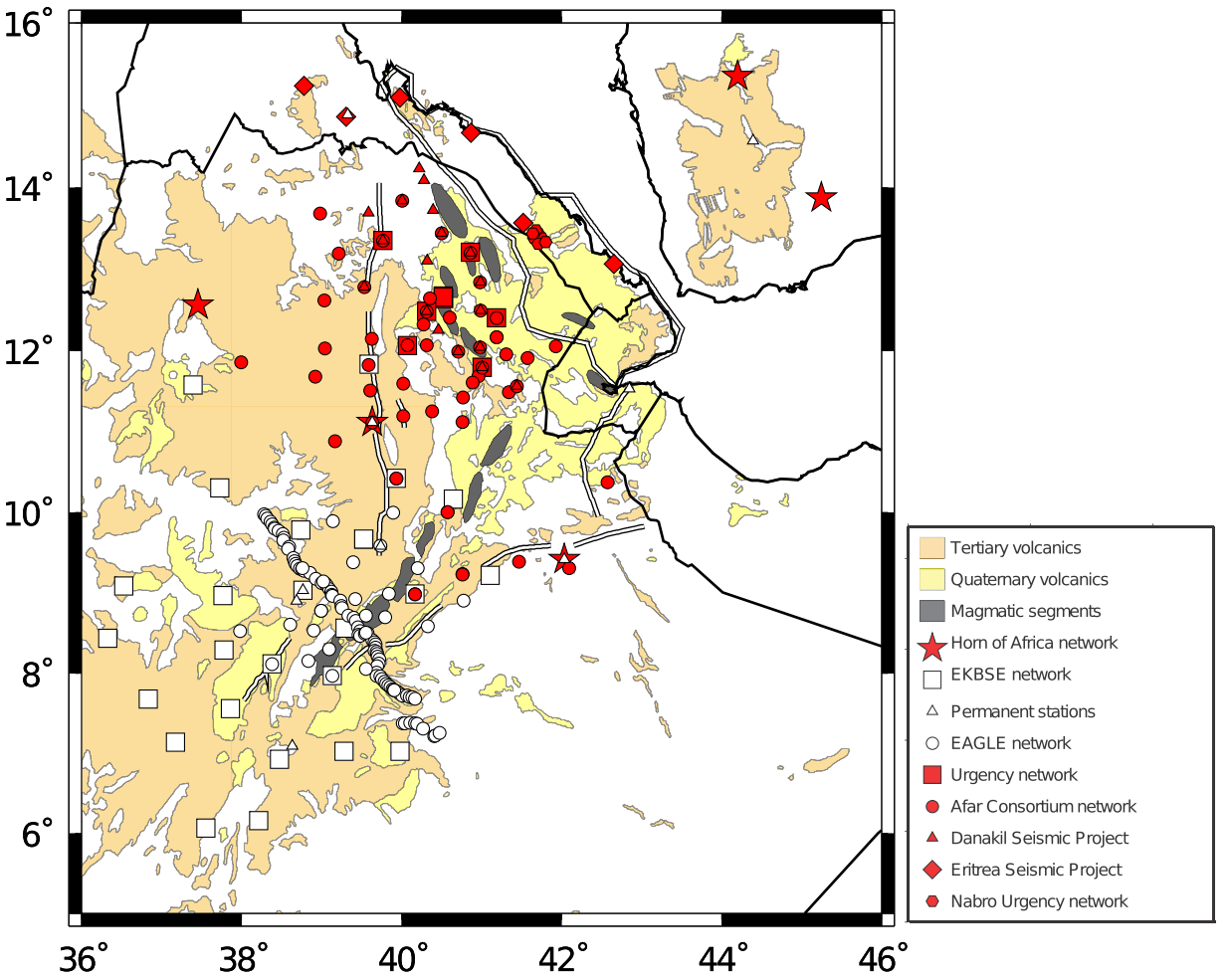

Figure 1. Map of the East Africa region showing Cenozoic flood basalt volcanism (Tertiary and Quaternary volcanics), currently active magmatic segments and border faults. All stations used in the study from recent seismic initiatives are also shown.

present day (Figure 1). Although some authors argue for a single plume located beneath Kenya and associated lateral flow of material in the upper mantle toward Ethiopia [*Ebinger and Sleep*, 1998; *Owens et al*., 2000; *Huerta et al*., 2009; *Hansen et al*., 2012; *Hansen and Nyblade*, 2013], other seismic tomographic images hint at low velocities beneath Afar extending into the lower mantle indicating the potential presence of an Afar plume [*Montelli et al*., 2006; *Chang and Van der Lee*, 2011]. However, to date, the spatial extent, morphology, and thermochemical nature of the lower-mantle African Superplume and its connectivity with the upper-mantle beneath East Africa remains unclear.

Incorporating new dense, high-quality data located across the Afar Triple Junction allows us to significantly improve our spatial coverage and hence our understanding of the geodynamical system beneath East Africa. Tomography and teleseismic receiver functions (RFs) provide evidence for ongoing upwelling across the MTZ that is likely driven, at least in part, by compositional buoyancy.

2. Data and Method

Earlier studies of MTZ structure beneath Ethiopia have been limited to the Main Ethiopian Rift (MER) and southernmost Afar due to the geographical distribution of stations associated with previous experiments [e.g., *Nyblade et al*., 2000b; *Benoit et al*., 2006b; *Cornwell et al*., 2011]. Incorporation of data from new seismic initiatives located throughout the Afar depression and Western Plateau have led to a significant

improvement in station coverage and opened the upper mantle in this region to detailed seismic investigation (Figure 1) [e.g., *Hammond et al*., 2013; *Rychert et al*., 2012].

The *S* wave seismic tomography model has been presented previously, where interpretations focused on the upper 400 km of the mantle [*Hammond et al*., 2013]. We present here for the first time the deeper parts of the *S* wave model (<700 km). Details of the inversion can be found in *Hammond et al*. [2013], but in summary, we include 13,161 S/SKS-wave travel time picks and invert the data using a standard regularized, linear least squares inversion [*VanDecar et al*., 1995], jointly inverting for slowness, near-surface corrections, and earthquake corrections. *Hammond et al*. [2013] show that resolution is excellent in the upper 400 km of the model beneath the study region. We have extended these checkerboard tests using the approach of *Hammond et al*. [2013], including normally distributed noise to the synthetic travel time data. These tests show that good resolution, sufficient to draw robust inferences, is also present to depths of 700 km beneath both the Main Ethiopian Rift and Afar Depression.

The new receiver function data set contains 5158 high-quality waveforms from 138 broadband seismic stations (Figure 2), between 2 and 4 times the data volume incorporated into previous RF studies of the MTZ beneath Ethiopia [*Benoit et al*., 2006b; *Cornwell et al*., 2011]. The RFs were calculated using the iterative time domain approach with a Gaussian pulse width of 0.625 [*Ligorria and Ammon*, 1999] and migrated to depth using a 3-D common conversion point method where the size of the stacking bins were determined by the Fresnel zone [*Wilson and Aster*, 2003; *Angus et al*., 2009; *Hammond et al*., 2011; *Thompson et al*., 2011]. A common slowness assumption (i.e., that the P-to-S conversions have the same slowness as the teleseismic *P* wave) was used in the 3-D migration, potentially leading to slight overestimates in MTZ thickness (maximum of 5 km, although as the mean epicentral distance of earthquakes used in this study is 73.8° it is unlikely to be more than 3 km) [*Lawrence and Shearer*, 2006]. A minimum RF amplitude of 0.005 was required for the arrivals from the MTZ discontinuities for a given stacking bin in order to use the observation to calculate MTZ thickness. Corrections for both crustal structure and upper-mantle velocity structure from the regional *P* and *S* wave tomographic models [*Hammond et al*., 2011, 2013] applied to the ak135 velocity model [*Kennett et al*., 1995] were also performed. Since the tomographic anomalies are relative to an undetermined background mean, absolute depths of the discontinuities are only indicative. However, there is good resolution of lateral variations in mantle velocity structure and MTZ thickness. We also migrate the data through the 1-D ak135 velocity model and, as did *Cornwell et al*. [2011], the global absolute *P* and *S* wave models of *Montelli et al*. [2006] for comparison.

In summary, the recent seismic deployments in the Afar Depression in combination with previous seismic experiments in the Main Ethiopian Rift (MER) [*Nyblade and Langston*, 2002; *Bastow et al*., 2011] provide unparalleled coverage and resolution at MTZ depths beneath this large igneous province both in terms of seismic tomography and RFs from the MTZ discontinuities (Figures 1 and 2). Furthermore, with the unique position of this purported plume locality being on land, data coverage and quality are superior to other extensively studied locales such as Hawaii or Iceland [*Wolfe et al*., 1997, 2009].

3. Results

3.1. Tomography

The *S* wave tomographic models show a persistent low-velocity zone (1–2% slow) throughout the transition zone beneath northern Afar (Figure 3). A second weaker anomaly is also present beneath the MER (Figure 3). It is unclear if this continues into the lower mantle as the models lose resolution at these depths. At the top of the transition zone, a broad anomaly is observed (Figure 3), similar to that shown for the uppermost mantle in *Hammond et al*. [2013]. These features are well resolved at depths extending to at least 600 km (Figure 4). More recent travel time inversions that extend the *Hammond et al*. [2013] models by including data from Tanzania and Saudi Arabia better constrain the velocity structure in the MTZ beneath the Horn of Africa (Civiero et al., Multiple mantle upwellings beneath the Northern East-African Rift System from relative P-wave traveltime tomography, submitted to *Earth and Planetary Science Letters*, 2015). They show extremely similar features within the MTZ, but with lower amplitudes.

3.2. Receiver Functions

The arrival times of P-to-S conversions from the MTZ discontinuities (*P*410*s* and *P*660*s*) relative to the direct *P* wave at a reference slowness of 6.5 s deg^{-1} are 49.2 ± 0.3 and 73.7 ± 0.9 s beneath northern Afar and

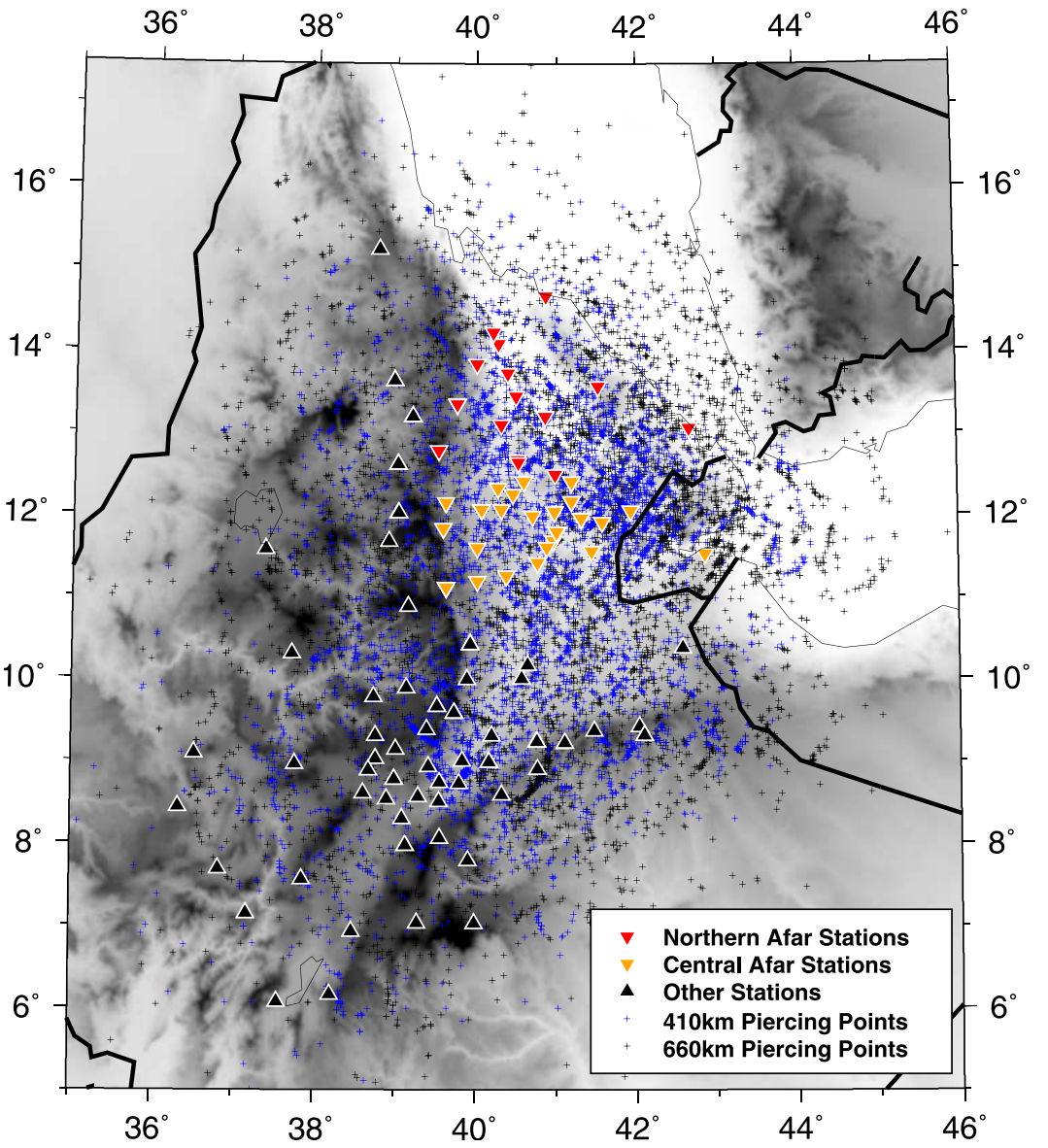

Figure 2. Data coverage for the receiver function data set in the form of piercing points at 410 and 660 km depth. Piercing points are calculated using the TauP toolkit [*Crotwell et al.*, 1999]. The densest data coverage is located in central and NE Afar, where subsequent transects through 42°E pass through.

49.2 ± 0.2 and 72.9 ± 0.3 s beneath central Afar, respectively (Figures 5 and 6; see Figure 2 for distribution of stations). These are consistently more than 5–6 s slow across the study region compared to that predicted by ak135 (43.9 and 67.9 s, respectively), making them some of the slowest *P*410*s* and *P*660*s* arrivals in the world along with Hawaii and Iceland [*Tauzin et al.*, 2008]. Despite these large delay times, mean differential arrival times (*P*660*s* - *P*410*s* = 24.5 ± 0.9 and 23.7 ± 0.3 s beneath northern and central Afar, respectively) closely correspond to that predicted by ak135 (24.03 s) and similar to several nonhot spot locations [*Tauzin et al.*, 2008]. This implies that, due to the similar paths taken in the upper mantle by both phases, most of the travel time anomaly is accrued above the *410*.

In the vicinity of the tomographically determined low-velocity anomaly seen beneath Afar, the MTZ thickness changes little (mean thickness of 251 km with standard deviation of 13 km determined from the 3-D migration, Figure 7) and lies close to, even slightly above, the global average (ranging from 242 to 247 km) [*Flanagan and Shearer*, 1998; *Gu and Dziewonski*, 2002; *Lawrence and Shearer*, 2006; *Tauzin et al.*, 2008]. This would argue against a significant temperature perturbation at MTZ depths across this region (certainly less

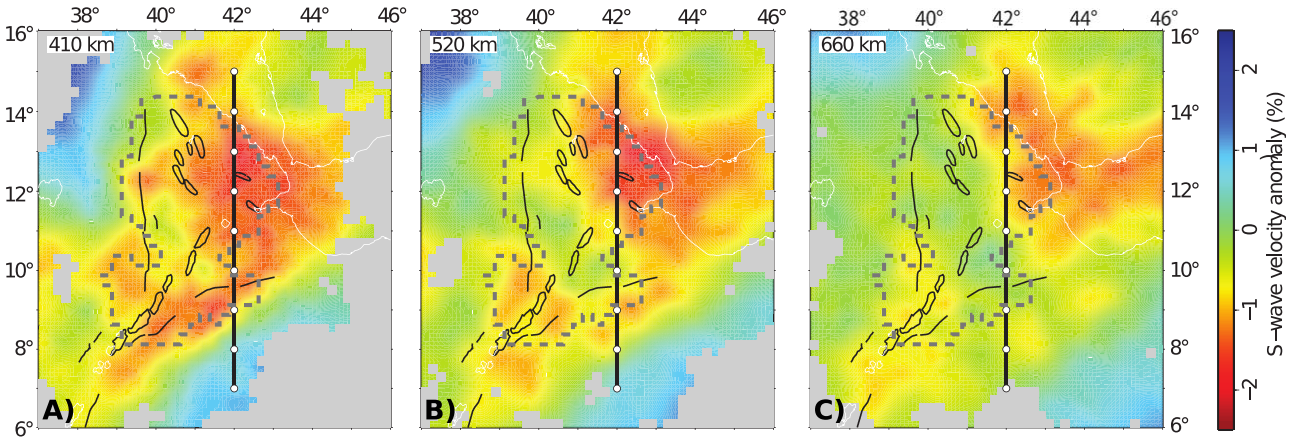

Figure 3. Slices through the *S* wave tomography model at depths of (a) 410 km, (b) 520 km, and (c) 660 km. At 410 km, a broader zone of low seismic velocities is apparent, while at 660 km depth, there is a focused region of reduced seismic velocities located beneath the eastern edge of the Afar region where the southern Red Sea meets the Gulf of Aden. The line is the N-S cross section shown in subsequent figures.

than 100 K) [*Helffrich*, 2000], consistent with previous single station observations [*Nyblade et al*., 2000a; *Benoit et al*., 2006a]. There are large perturbations to the apparent topography and MTZ thickness in regions characterized by rapid lateral changes in upper-mantle velocity structure and anisotropy [*Hammond et al*., 2011, 2013, 2014; *Kendall et al*., 2005; *Gao et al*., 2010; *Rychert et al*., 2012; *Bastow et al*., 2008], i.e., the border fault regions in Figure 7 where the MER opens into the Afar triangle (∼9°, 40°E). Rapid changes in structure were also seen by *Cornwell et al*. [2011]; however, this is in a region where we observe incoherent stacking of the signal (note the reduction in amplitude of the *410* and the apparently diffuse *660* at the southern edge of Figure 8 and in the vicinity of the southern border faults in Figures S1–S3) and choose to focus our interpretation on Afar where the crust, lithosphere, and upper-mantle structure is more coherent.

Despite the lack of evidence for MTZ thinning associated with the tomographic anomaly beneath Afar, the RF waveforms show evidence for a negative conversion above the *410* irrespective of the velocity model used for migration (Figures 5–8 and S1–S4). This implies the presence of a distinct, depth-localized low-velocity layer (LVL) above the *410*, which is most pronounced where the lowest seismic velocity anomalies are observed in the tomography (Figures 7 and 8). A similar LVL has been previously observed in diverse tectonic settings globally including beneath station ATD in Djibouti [*Tauzin et al*., 2010], but our study maps its detailed spatial extent beneath Afar for the first time. A number of features in the RF data show that this is a robust observation. The arrival from the top of the LVL exhibits positive moveout with slowness (Figures 5 and 6), indicative of direct P-to-S conversions as opposed to reverberations from shallower discontinuities. It is not an artifact of the RF estimation technique [*Ligorria and Ammon*, 1999] because there is no symmetric side lobe of comparable amplitude on the underside of the *410* (Figures 5 and 6). Moreover, the ray sampling is densest here, making results from northern and central Afar extremely robust (Figure 2). Although anomalously slow, the crust and upper-mantle structure across much of Afar is relatively uniform [*Hammond et al*., 2011, 2013] with little anisotropy compared to the MER [*Hammond et al*., 2014], resulting in the migrated RF signal stacking coherently (Figures 8 and S1–S4). The approximate spatial extent of the LVZ, estimated from its robust amplitude detection from the crust and upper-mantle corrected 3-D CCP migration (Figure S3), is shown in Figure 7.

4. Discussion

Seismic tomography, especially in the case where surface-waves are not used, can result in significant vertical smearing. Therefore, the presence of a LVL above the *410* could contribute to the low seismic velocities within the MTZ. Figure S5 shows a synthetic test where a 4% slow, 60 km thick low-velocity layer sits directly above the *410* [e.g., *Tauzin et al*., 2010]. It is evident that such a thin layer is not resolvable by tomography alone and that smearing occurs, but it is not of significant amplitude to explain the observed anomaly (Figure S5). This suggests that there must still be reduced seismic velocities within the MTZ beneath Afar to

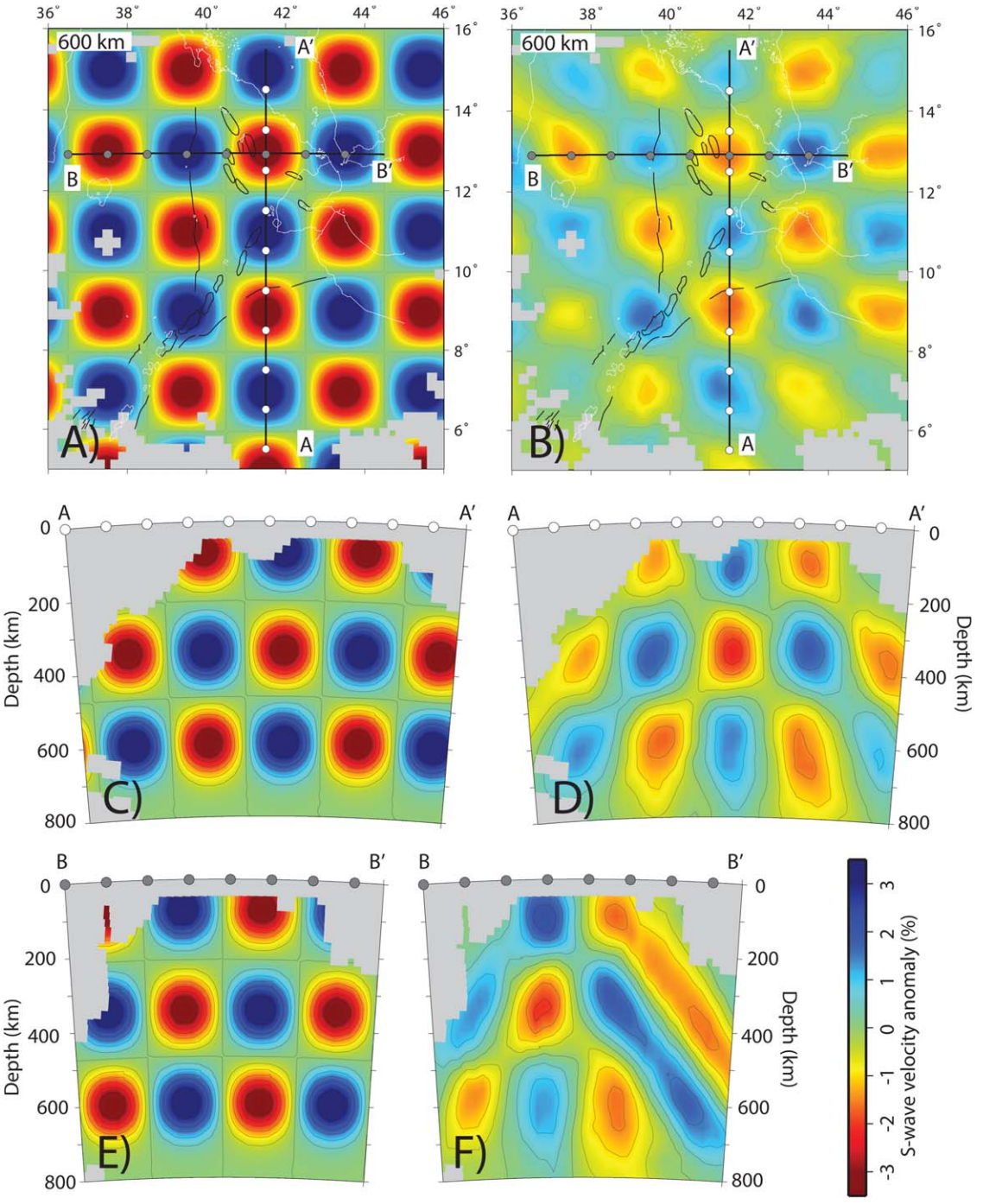

Figure 4. Checkerboard resolution test for the teleseismic *S* wave tomographic inversions. The input model consists of alternating positive and negative anomalies with magnitude of 4% every 2° laterally and at depths of 100, 350, and 600 km. Map views through the (a) input and (b) recovered models at 600 km depth. N-S cross sections for the (c) input and (d) recovered velocity models, and E-W cross sections through the (e) synthetic and (f) recovered model.

explain the observations. The simplest way to explain this is through the presence of a warm thermal anomaly. There has been much debate over the strength of any thermal anomaly in the upper mantle beneath the Afar Depression. *Cornwell et al*. [2011], based on MTZ structure from the MER and southern Afar, suggested a thermal anomaly of +250 K beneath the region. Alternatively, *S* wave receiver functions suggest that little anomaly is required [*Rychert et al*., 2012], but recent geochemical analyses and petrological

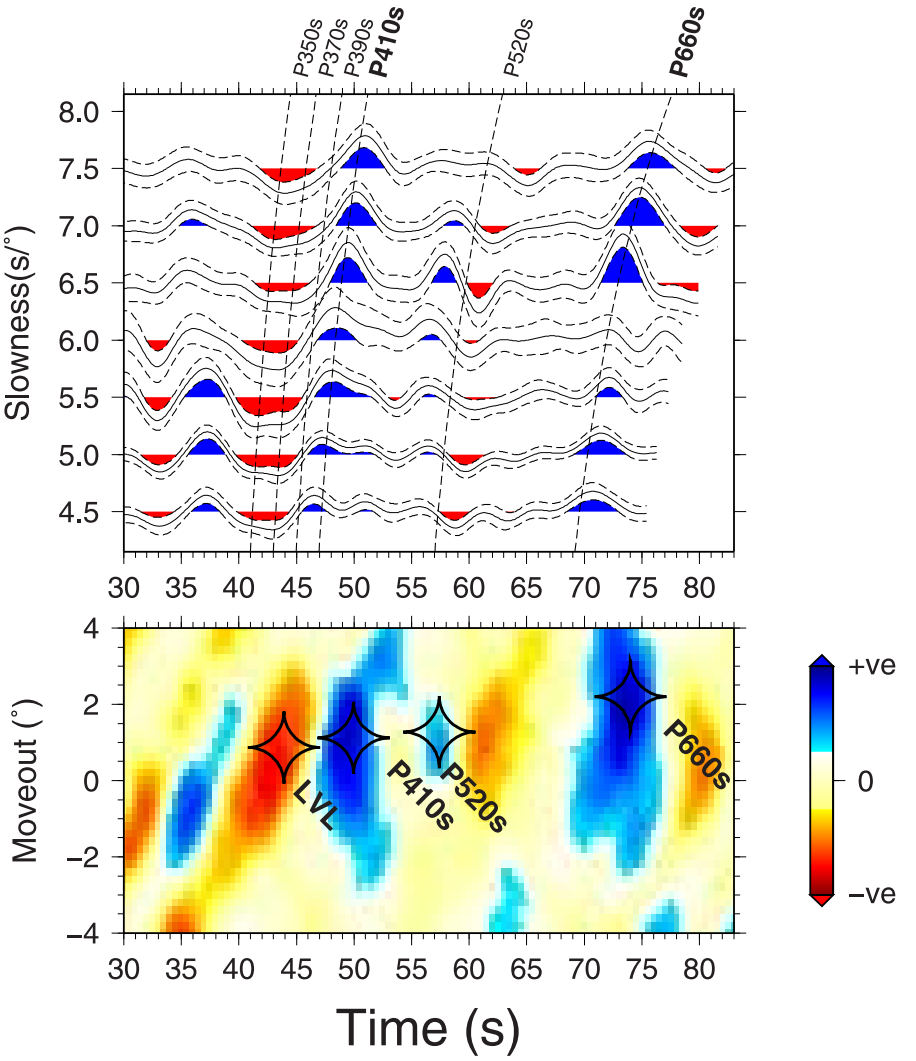

Figure 5. (top) Receiver functions binned by slowness for Northern Afar. The size of the bins are 1 s deg^{-1} with 50% overlap between bins meaning that each receiver function contributes to 2 bins. For each bin, the receiver functions are moveout corrected to the slowness at the center of the bin and linearly stacked to produce the presented trace. The dashed traces are the 2σ confidence bounds of the stacked traces. The labeled dashed lines are the predicted moveout curves for various seismic phases delayed by 6 s compared to the theoretical values in order to correct for the time delay due to velocity anomalies in the upper mantle. (bottom) Slant stacks of the receiver functions using an nth root stacking regime (4th root) [*McFadden et al.*, 1986].

constraints suggest an excess temperature of +100 to 150 K [*Rooney et al.*, 2012; *Ferguson et al.*, 2013]. Based on our estimates of TZ thickness from across Afar, +150 K appears too high as we would expect to see significant variations in MTZ thickness associated with this, but a thermal anomaly of <100 K is consistent with our results. This observation is supported by recent estimates from *P* wave tomography and joint seismic, geochemical, and numerical modeling that suggest a mild thermal anomaly of ~100 K exists in the MTZ and upper mantle beneath the Afar Depression(Armitage et al., Upper mantle temperature and the onset of extension and break-up in Afar, Africa, submitted to *Earth and Planetary Science Letters*, 2015; Civiero et al., submitted manuscript, 2015). To test this, we build a synthetic model that mimics a broad, ~100 K anomaly in the mantle, together with the melt layer. The 100 K anomaly has ~1.5% anomaly above the transition zone and ~0.5% anomaly within the transition zone [*Styles et al.*, 2011; Civiero et al., submitted manuscript, 2015]. This simple model is consistent with the tomography model (Figures 7, 8, and S6). Amplitudes are still lower than that seen in the data inversions; however, Figure S7 shows a case where we increase the velocity contrast associated with the melt layer. It is clear that, while the vertical extent of the melt layer is not constrained by the tomography alone, the melt layer can play a controlling influence on the amplitudes recovered in the model. However, given that shallow low-velocity anomalies are also likely

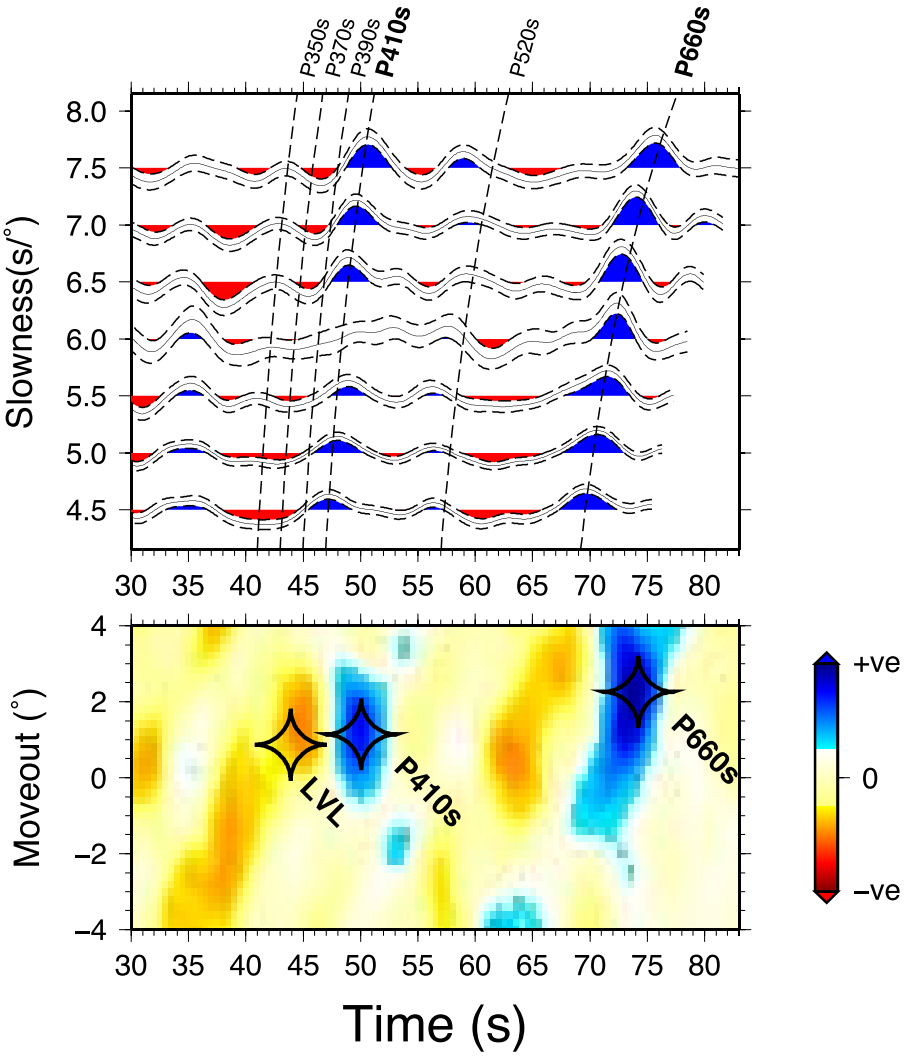

Figure 6. Slowness stacks and slant stacking for Central Afar. Plotting convention follows Figure 5.

smeared deeper, care must be taken when interpreting the amplitudes of the anomalies within the MTZ (Civiero et al., submitted manuscript, 2015). Despite this, it is important that the lowest seismic velocities imaged from tomography beneath Afar coincide with the presence of a stable melt layer imaged using the RFs.

A low-velocity layer above the *410* is commonly ascribed to a stable, depth-localized region of partial melt [*Revenaugh and Sipkin*, 1994]. It is difficult to reconcile the depth-localized nature of this feature using elevated temperature alone [*Tauzin et al.*, 2010], consistent with our MTZ thickness estimates. Other mechanisms are often invoked, most notably the presence of water. Recent observations have confirmed that the MTZ can be locally hydrated, containing up to 1.5 wt % water [*Pearson et al.*, 2014]. Within the upper part of the MTZ, water storage capacity of wadsleyite is expected to be 5 times what it is above the *410* [*Inoue et al.*, 2010], meaning upwelling material transforming into olivine has the potential to exceed the upper-mantle water storage capacity and induce partial melting [*Hirschmann*, 2006]. This so-called transition zone water filter model [*Bercovici and Karato*, 2003] predicts a global LVL above the *410* due to the passive upwelling of ambient mantle, a conclusion that some seismic results support [*Tauzin et al.*, 2010]. The original model also predicts that this process would be suppressed in plume-affected regions due to increased water solubility with increasing temperature and short residence times in the MTZ [*Bercovici and Karato*, 2003]. These predictions have been questioned recently, instead suggesting that ambient mantle (the expected source of mid-ocean ridge basalt) does not have sufficient water content (<200 ppm) to exceed

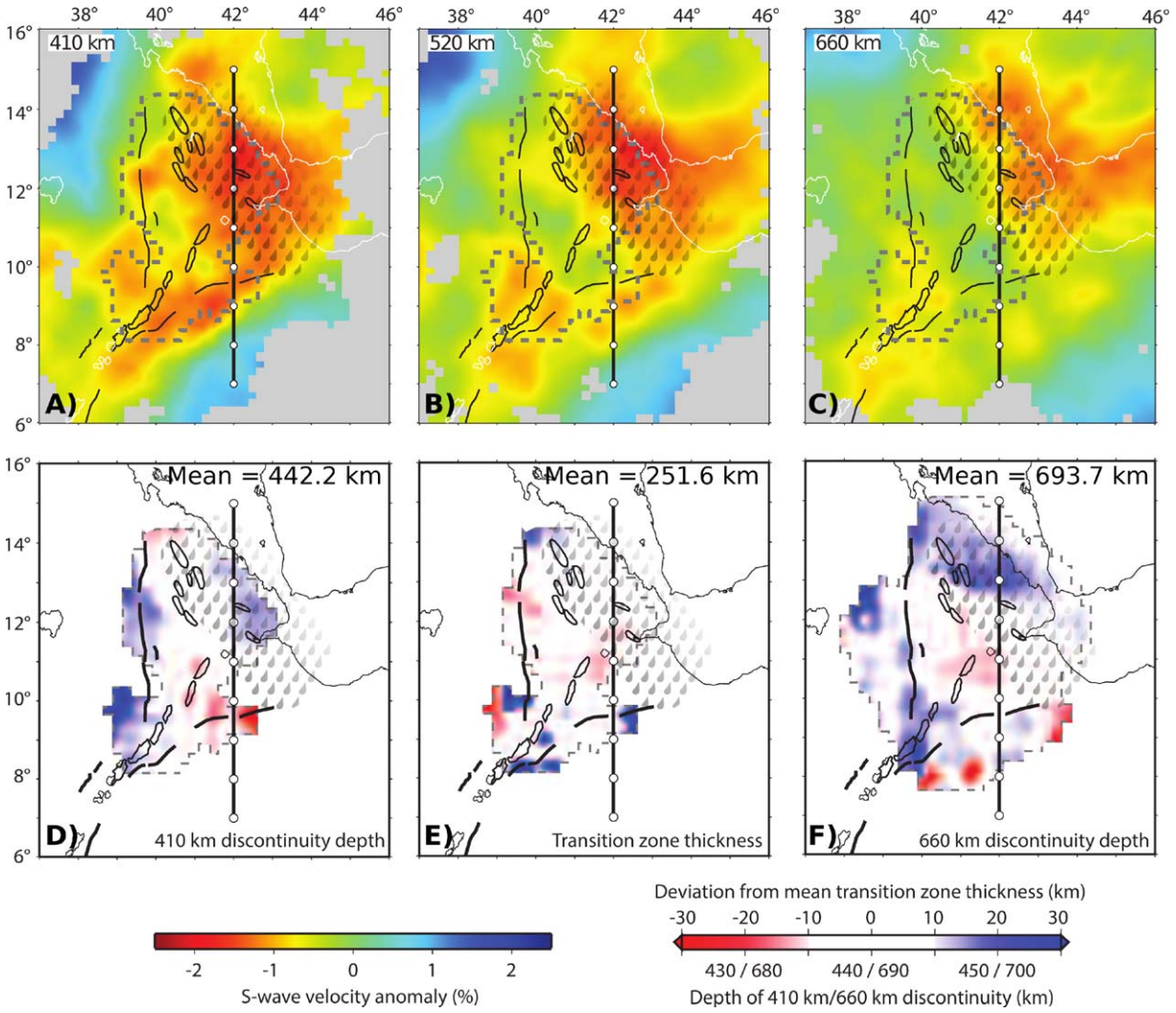

Figure 7. (a–c) Slices through the *S* wave tomography model at 410, 520, and 660, respectively (see Figure 3). (d–f) Apparent topography of the *410*, MTZ thickness and apparent topography of the *660*. Regions of anomalous MTZ thickness can be seen coincident with the MER and other border faults where rapid changes in upper-mantle velocity structure and anisotropy are present. The line of cross section is 42°E. The dashed region is the limit of CCP bins with 150 hits per bin, and the region with shaded droplets is the approximate extent of the LVL determined by its detection in the 3-D CCP migration.

the upper-mantle storage capacity directly above the *410*, even with the reduced values predicted by the most recent studies (440–850 ppm) [*Tenner et al*., 2012; *Férot and Bolfan-Casanova*, 2012]. Thus, a global LVL may not be present. In contrast, plume source mantle has been shown to have sufficiently high water content (up to 1000 ppm) to significantly exceed the upper-mantle storage capacity [*Nichols et al*., 2002]. This would permit the formation of a localized melt layer [*Tenner et al*., 2012], as is seen here, without recourse to a global model that is controversial as to the amount of water assumed to be in normal mantle. An associated broadening of the *410* may also be expected [*Frost and Dolejs*, 2007], but the presence of a pronounced LVL above the discontinuity complicates observation of this broadening through its amplitude. The presence of melt may also act to truncate the region of coexistence between olivine and wadsleyite [*Helffrich*, 2000], creating a sharper than expected seismic discontinuity.

Our results provide some of the most compelling and well-constrained evidence to date for the formation of this melt layer in the presence of currently active upwelling in a volcanic environment. Such low-velocity layers have been found beneath some other Mesozoic flood basalts [*Vinnik and Farra*, 2007], yet this spatial correlation requires the controversial assumption of long-term coupling of the continental lithosphere and

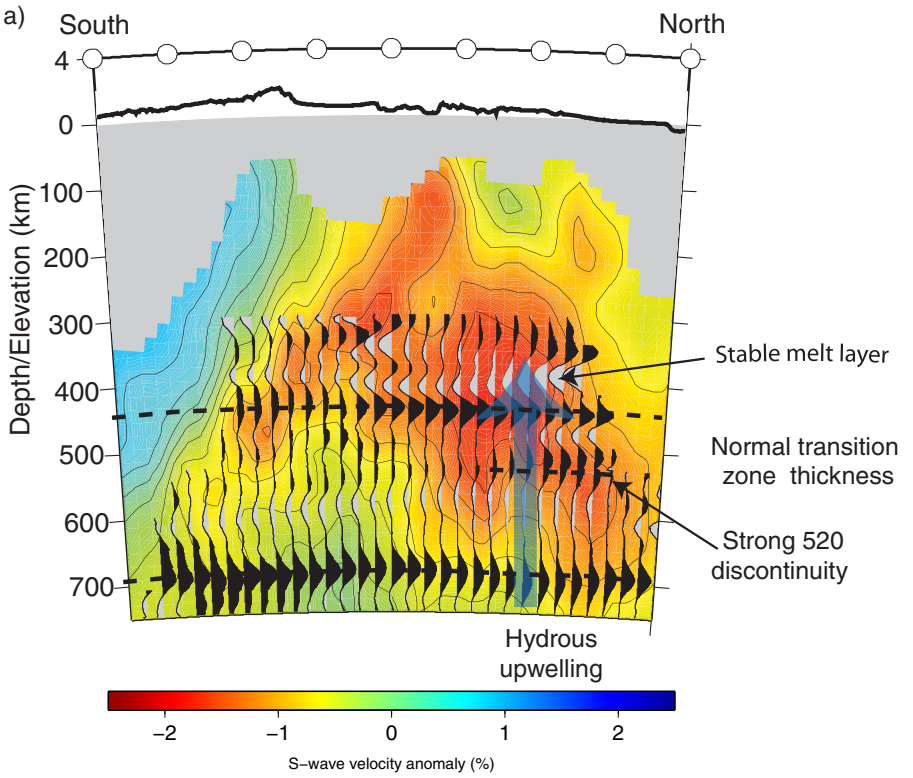

Figure 8. Cross section including surface topography showing correlation between low seismic velocities from the teleseismic travel time tomography (*S* wave velocity perturbations in the background) [*Hammond et al.*, 2013], the LVL above *410* and the prominent *520* from RF analysis. A hydrous upwelling from the lower mantle best reconciles the observed, coincident features.

underlying mantle to depths ~400 km. A LVL has also been recently suggested beneath Hawaii in conjunction with a significant depression of the *410* (from 400 to 450 km, interpreted as a temperature anomaly of >300K [*Huckfeldt et al.*, 2013]). The results from Afar are novel for the fact that no significant variation in discontinuity depth or MTZ thickness is correlated with it. Consistent with the latest tomographic studies (Civiero et al., submitted manuscript, 2015), this suggests that only a weak thermal anomaly (<100 K) can be invoked to drive upwelling beneath northern and central Afar. Hydration can also contribute to positive buoyancy, with the addition of ~2000 ppm water having the same effect on the density of olivine as a temperature increase of 100 K [*Smyth et al.*, 2006]. With upwelling of hydrous mantle being a fundamental requirement to initiate dehydration melting on top of the *410*, it must be driven in part by compositional buoyancy beneath the Afar Triple Junction. Volcanics from the study region have suggested a volatile-rich and hydrous source for metasomatism of the lithospheric mantle [*Baker et al.*, 1998], and the origins of the upwelling may lie with recycled, metasomatized subducted oceanic lithospheric mantle, explaining both the hydrous and compositionally buoyant nature of the inferred upwelling [*Niu and O'Hara*, 2003; *Niu et al.*, 2012].

Compositional buoyancy has been suggested beneath East Africa previously, but in terms of negative buoyancy at depths of ~1000 km [*Simmons et al.*, 2007]. This is below where we have resolution, so cannot confirm or refute the presence of this feature. However, complex geodynamics are expected in the lower mantle in the presence of recycled, compositionally layered oceanic lithosphere and/or a dense basal layer at the bottom of the mantle [*Tackley*, 2011; *Olson and Kincaid*, 1991], hence our interpretations are not necessarily contradictory.

In association with the LVL, there is also a strong positive polarity arrival within the MTZ beneath northern Afar that we interpret as the *520* seismic discontinuity (Figures 5, 6, and 8), an arrival not commonly observed in higher-frequency RF studies. As with the conversion from the top of the LVL, the moveout characteristics of the *520* indicate a direct P-to-S conversion (Figures 5 and 6). The width of the two-phase loop associated with this discontinuity is expected to shrink under hydrous conditions, producing a stronger converted seismic signal [*Inoue et al.*, 2010]. The *520* appears more visible where the LVL is at its thickest and

the low-velocity anomaly in the tomography is at its greatest (Figure 8), providing further evidence for localized hydration of the mantle. There appears to be a doubling of the *520* in the migrated RFs beneath northern Afar (Figure 8), but this is likely due to the stacking of a single discontinuity with laterally variable depths. With water expected to alter the depth of the *520*, it is plausible that the variability in depth is also related to water content [*Inoue et al*., 2010]. A recent study of the *520* beneath the African continent, incorporating data from station ATD, also attests to the variability of this discontinuity beneath our study region [*Julià and Nyblade*, 2013].

While we try to avoid interpreting the more subtle features of our models, there appears to be a minor thickening of the MTZ due to a depression of the 660 moving from central into northern Afar (the location of the tomographically determined low-velocity anomaly, Figure 8). Assuming the dominance of the olivine system under anhydrous conditions, this is opposite to what would be expected for a hot mantle [*Helffrich*, 2000]. While the depth of the *410* is expected to be relatively unaffected by the presence of water ($<$5 km variation over plausible mantle water contents) [*Frost and Dolejs*, 2007], recent work has suggested that the depth of the *660* could be more sensitive to it (potentially up to 40 km deeper than under anhydrous conditions) [*Ghosh et al*., 2013]. Therefore, this feature may also be consistent with a hydrous MTZ. Another explanation for this feature is that high temperatures can lead to the *660* region being controlled by the garnet to perovskite phase transition [*Weidner and Wang*, 1998], with an opposite Clapeyron slope to that of the ringwoodite to perovskite transition. This would imply an increase in temperature could in fact cause a deepening of the *660* and a relatively normal, or even increased, MTZ thickness [*Deuss*, 2007]. For example, *Cornwell et al*. [2011] interpreted variations in bulk composition (i.e., variations in the amount of garnet) within a ubiquitously hot mantle ($+$250 K) to explain the strong variations in MTZ thickness observed beneath the MER. As stated previously, we choose to confine our interpretations to the Afar region where the stacking coherence is high. Due to the lack of any correlated topography on the *410* associated with the deepening of the *660* and the latest tomographic studies consistent with only a mild temperature elevation ($\sim$100 K) (Civiero et al., submitted manuscript, 2015), we discard phase changes associated with the garnet system at high temperature as a viable interpretation for this feature.

We showed that compositional buoyancy, whose source lies in the lower mantle, must play a role in the development of the seismic structure below Ethiopia. Various observations of isotopic and major element heterogeneity in East African lavas [*Pik et al*., 2006; *Meshesha and Shinjo*, 2008] suggest compositional variability of their sources, some of which are inferred to lie in the lower mantle. Our results support both the inference of a deep source (certainly beneath the *410*), and also the extreme heterogeneity. *Duncan and Richards* [1991] showed that compositional buoyancy diminishes mixing by entrainment, leading to juxtaposed compositions arising from different sources. We speculate that the surface chemistry of Afar rocks may map lower-mantle source chemistry.

5. Conclusions

The new high-resolution images of the MTZ constrain upwelling beneath the Afar Triple Junction. The RF data and seismic tomography show that only a weak thermal gradient is required in the MTZ across East Africa, but small, volatile-rich, and compositionally buoyant plumelets which rise through the MTZ from a heterogeneous deep mantle source likely exist. It is these plumelets that give rise to the complex geochemical signatures observed across Ethiopia and East Africa, and when sufficiently hydrous lead to the formation of a stable melt layer above the *410*. The results show that mantle plumes maybe more complex than previously thought, and that in some regions are likely driven by differences in composition rather than temperature alone. This is an important consideration not just for East Africa, but in understanding how mantle plumes interact with the MTZ and the transport of chemical heterogeneity from the deep Earth.

Acknowledgments
We would like to thank Addis Ababa University, Eritrea Institute of Technology, the Afar National Regional State Government, Ethiopia, and the Southern Red Sea Region Administration, Eritrea for support throughout the various experiments. The facilities of SEIS-UK are supported by the Natural Environment Research Council under agreement R8/H10/64. Seismic instruments were also supplied by IRIS-PASSCAL. The facilities of the IRIS Consortium are supported by the National Science Foundation under Cooperative agreement EAR-0552316 and by the Department of Energy National Nuclear Security Administration. Funding was provided by NERC grants NE/E007414/1, NE/D008611/1, and NE/J012297/1, NSF grant EAR-0635789, and BHP-Billiton. J.O.S.H. was supported by NERC Fellowship NE/I020342/1. All data are available through the Incorporated Research Institutions for Seismology (IRIS) Data Management Centre (DMC). We thank two anonymous reviewers for constructive comments that improved the clarity of the paper.

References

Angus, D. A., J.-M. Kendall, D. C. Wilson, D. J. White, S. Sol, and C. J. Thomson (2009), Stratigraphy of the Archean western Superior Province from P-and S-wave receiver functions: Further evidence for tectonic accretion?, *Phys. Earth Planet. Inter.*, *177*(3–4), 206–216, doi:10.1016/j.pepi.2009.09.002.

Baker, J., G. Chazot, M. Menzies, and M. Thirlwall (1998), Metasomatism of the shallow mantle beneath Yemen by the Afar plume—Implications for mantle plumes, flood volcanism, and intraplate volcanism, *Geology*, *26*(5), 431–434.

Bastow, I. D., A. Nyblade, G. W. Stuart, T. O. Rooney, and M. H. Benoit (2008), Upper mantle seismic structure beneath the Ethiopian hot spot: Rifting at the edge of the African low-velocity anomaly, *Geochem. Geophys. Geosyst.*, *9*, Q12022, doi:10.1029/2008GC002107.

Bastow, I. D., D. Keir, and E. Daly (2011), The Ethiopia Afar Geoscientific Lithospheric Experiment (EAGLE): Probing the transition from continental rifting to incipient seafloor spreading, *Volcanism Evol. Afr. Lithosphere*, *478*, 51–76.
Beier, C., T. Rushmer, and S. P. Turner (2008), Heat sources for mantle plumes, *Geochem. Geophys. Geosyst.*, *9*, Q06002, doi:10.1029/2007GC001933.
Benoit, M. H., A. A. Nyblade, T. J. Owens, and G. W. Stuart (2006a), Mantle transition zone structure and upper mantle S velocity variations beneath Ethiopia: Evidence for a broad, deep-seated thermal anomaly, *Geochem. Geophys. Geosyst.*, *7*, Q11013, doi:10.1029/2006GC001398.
Benoit, M. H., A. A. Nyblade, and J. C. VanDecar (2006b), Upper mantle P-wave speed variations beneath Ethiopia and the origin of the Afar hotspot, *Geology*, *34*(5), 329–332.
Bercovici, D., and S. Karato (2003), Whole-mantle convection and the transition-zone water filter, *Nature*, *425*(6953), 39–44.
Chang, S. J., and S. Van der Lee (2011), Mantle plumes and associated flow beneath Arabia and East Africa, *Earth Planet. Sci. Lett.*, *302*, 448–454.
Cornwell, D. G., G. Hetényi, and T. D. Blanchard (2011), Mantle transition zone variations beneath the Ethiopian Rift and Afar: Chemical heterogeneity within a hot mantle?, *Geophys. Res. Lett.*, *38*, L16308, doi:10.1029/2011GL047575.
Crotwell, H. P., T. J. Owens, and J. Ritsema (1999), The TauP Toolkit: Flexible seismic travel-time and ray-path utilities, *Seismol. Res. Lett.*, *70*(2), 154–160, doi:10.1785/gssrl.70.2.154.
Deuss, A. (2007), Seismic observations of transition zone discontinuities beneath hotspot locations, *Spec. Pap. Geol. Soc. Am.*, *430*, 121–136.
Duncan, R. A., and M. A. Richards (1991), Hotspots, mantle plumes, flood basalts, and true polar wander, *Rev. Geophys.*, *29*(1), 31–50.
Ebinger, C. J., and N. H. Sleep (1998), Cenozoic magmatism throughout east Africa resulting from impact of a single plume, *Nature*, *395*(6704), 788–791.
Ferguson, D. J., J. Maclennan, I. D. Bastow, D. M. Pyle, D. Keir, J. D. Blundy, T. Plank, and G. Yirgu (2013), Melting during late-stage rifting in Afar is hot and deep, *Nature*, *499*, 70–73, doi:10.1038/nature12292.
Férot, A., and N. Bolfan-Casanova (2012), Water storage capacity in olivine and pyroxene to 14GPa: Implications for the water content of the Earth's upper mantle and nature of seismic discontinuities, *Earth Planet. Sci. Lett.*, *349*, 218–230.
Flanagan, M. P., and P. M. Shearer (1998), Global mapping of topography on transition zone velocity discontinuities by stacking SS precursors, *J. Geophys. Res.*, *103*(B2), 2673–2692.
Frost, D. J., and D. Dolejs (2007), Experimental determination of the effect of H_2O on the 410-km seismic discontinuity, *Earth Planet. Sci. Lett.*, *256*(1-2), 182–195.
Gao, S. S., K. H. Liu, and M. G. Abdelsalam (2010), Seismic anisotropy beneath the Afar Depression and adjacent areas: Implications for mantle flow, *J. Geophys. Res.*, *115*, B12330, doi:10.1029/2009JB007141.
Ghosh, S., E. Ohtani, K. D. Litasov, A. Suzuki, D. Dobson, and K. Funakoshi (2013), Effect of water in depleted mantle on post-spinel transition and implication for 660km seismic discontinuity, *Earth Planet. Sci. Lett.*, *371–372*, 103–111, doi:10.1016/j.epsl.2013.04.011.
Gu, Y. J., and A. M. Dziewonski (2002), Global variability of transition zone thickness, *J. Geophys. Res.*, *107*(B7), 2135, doi:10.1029/2001JB000489.
Hammond, J. O. S., J.-M. Kendall, G. W. Stuart, D. Keir, C. Ebinger, A. Ayele, and M. Belachew (2011), The nature of the crust beneath the Afar triple junction: Evidence from receiver functions, *Geochem. Geophys. Geosyst.*, *12*, Q12004, doi:10.1029/2011GC003738.
Hammond, J. O. S., J.-M. Kendall, G. W. Stuart, C. J. Ebinger, I. D. Bastow, D. Keir, A. Ayele, B. Goitom, G. Ogubazghi, and T. J. Wright (2013), Mantle upwelling and initiation of rift segmentation beneath the Afar Depression, *Geology*, *41*, 635–638, doi:10.1130/G33925.1.
Hammond, J. O. S., J.-M. Kendall, J. Wookey, G. W. Stuart, D. Keir, and A. Ayele (2014), Differentiating flow, melt, or fossil seismic anisotropy beneath Ethiopia, *Geochem. Geophys. Geosyst.*, *15*, 1878–1894, doi:10.1002/2013GC005185.
Hansen, S. E., and A. A. Nyblade (2013), The deep seismic structure of the Ethiopia/Afar hotspot and the African superplume, *Geophys. J. Int.*, *194*(1), 118–124.
Hansen, S. E., A. A. Nyblade, and M. H. Benoit (2012), Mantle structure beneath Africa and Arabia from adaptively parameterized P-wave tomography: Implications for the origin of Cenozoic Afro-Arabian tectonism, *Earth Planet. Sci. Lett.*, *319*, 23–34.
Helffrich, G. (2000), Topography of the transition zone seismic discontinuities, *Rev. Geophys.*, *38*(1), 141–158.
Hirschmann, M. M. (2006), Water, melting, and the deep Earth H_2O cycle, *Annu. Rev. Earth Planet. Sci.*, *34*, 629–653, doi:10.1146/annurev.earth.34.031405.125211.
Huckfeldt, M., A. M. Courtier, and G. M. Leahy (2013), Implications for the origin of Hawaiian volcanism from a converted wave analysis of the mantle transition zone, *Earth Planet. Sci. Lett.*, *373*, 194–204, doi:10.1016/j.epsl.2013.05.003.
Huerta, A. D., A. A. Nyblade, and A. M. Reusch (2009), Mantle transition zone structure beneath Kenya and Tanzania: More evidence for a deep-seated thermal upwelling in the mantle, *Geophys. J. Int.*, *177*(3), 1249–1255, doi:10.1111/j.1365-246X.2009.04092.x.
Inoue, T., T. Wada, R. Sasaki, and H. Yurimoto (2010), Water partitioning in the Earth's mantle, *Phys. Earth Planet. Inter.*, *183*(1), 245–251.
Ito, G., and P. E. van Keken (2007), Hotspots and melting anomalies, *Treatise Geophys.*, *7*, 371–436.
Julià, J., and A. A. Nyblade (2013), Probing the upper mantle transition zone under Africa with P520s conversions: Implications for temperature and composition, *Earth Planet. Sci. Lett.*, *368*, 151–162, doi:10.1002/2013GC005186.
Kendall, J.-M., G. W. Stuart, C. J. Ebinger, I. D. Bastow, and D. Keir (2005), Magma-assisted rifting in Ethiopia, *Nature*, *433*(7022), 146–148.
Kennett, B. L. N., E. R. Engdahl, and R. Buland (1995), Constraints on seismic velocities in the Earth from traveltimes, *Geophys. J. Int.*, *122*(1), 108–124.
Lawrence, J. F., and P. M. Shearer (2006), A global study of transition zone thickness using receiver functions, *J. Geophys. Res.*, *111*, B06307, doi:10.1029/2005JB003973.
Ligorria, J. P., and C. J. Ammon (1999), Iterative deconvolution and receiver-function estimation, *Bull. Seismol. Soc. Am.*, *89*(5), 1395–1400.
McFadden, P. L., B. J. Drummond, and S. Kravis (1986), The N th-root stack: Theory, applications, and examples, *Geophysics*, *51*(10), 1879–1892.
Meshesha, D., and R. Shinjo (2008), Rethinking geochemical feature of the Afar and Kenya mantle plumes and geodynamic implications, *J. Geophys. Res.*, *113*, B09209, doi:10.1029/2007JB005549.
Montelli, R., G. Nolet, F. A. Dahlen, and G. Masters (2006), A catalogue of deep mantle plumes: New results from finite-frequency tomography, *Geochem. Geophys. Geosyst.*, *7*, Q11007, doi:10.1029/2006GC001248.
Morgan, W. J. (1971), Convection Plumes in the Lower Mantle, *Nature*, *230*, 42–43, doi:10.1038/230042a0.
Nichols, A. R. L., M. R. Carroll, and A. Höskuldsson (2002), Is the Iceland hot spot also wet? Evidence from the water contents of undegassed submarine and subglacial pillow basalts, *Earth Planet. Sci. Lett.*, *202*(1), 77–87.
Niu, Y., and M. J. O'Hara (2003), Origin of ocean island basalts: A new perspective from petrology, geochemistry, and mineral physics considerations, *J. Geophys. Res.*, *108*(B4), 2209, doi:10.1029/2002JB002048.

Niu, Y., M. Wilson, E. R. Humphreys, and M. J. O'Hara (2012), A trace element perspective on the source of ocean island basalts (OIB) and fate of subducted ocean crust (SOC) and mantle lithosphere (SML), *Episodes*, *35*(2), 310–327.
Nyblade, A. A., and C. A. Langston (2002), Broadband seismic experiments probe the East African rift, *EOS Trans. AGU*, *83*(37), 405–409.
Nyblade, A. A., R. P. Knox, and H. Gurrola (2000a), Mantle transition zone thickness beneath Afar: Implications for the origin of the Afar hotspot, *Geophys. J. Int.*, *142*(2), 615–619.
Nyblade, A. A., T. J. Owens, H. Gurrola, J. Ritsema, and C. A. Langston (2000b), Seismic evidence for a deep upper mantle thermal anomaly beneath east Africa, *Geology*, *28*(7), 599–602.
Olson, P., and C. Kincaid (1991), Experiments on the interaction of thermal convection and compositional layering at the base of the mantle, *J. Geophys. Res.*, *96*(B3), 4347–4354.
Owens, T. J., A. A. Nyblade, H. Gurrola, and C. A. Langston (2000), Mantle transition zone structure beneath Tanzania, East Africa, *Geophys Res. Lett.*, *27*(6), 827–830.
Pearson, D. G., et al. (2014), Hydrous mantle transtion zone indicated by ringwoodite included within diamond, *Nature*, *507*, 221–224, doi: 10.1038/nature13080.
Pik, R., B. Marty, and D. R. Hilton (2006), How many mantle plumes in Africa? The geochemical point of view, *Chem. Geol.*, *226*(3), 100–114.
Revenaugh, J., and S. A. Sipkin (1994), Seismic evidence for silicate melt atop the 410-km mantle discontinuity, *Nature*, *369*(6480), 474–476.
Rooney, T. O., C. Herzberg, and I. D. Bastow (2012), Elevated mantle temperature beneath East Africa, *Geology*, *40*(1), 27–30.
Rychert, C. A., J. O. S. Hammond, N. Harmon, J.-M. Kendall, D. Keir, C. J. Ebinger, I. D. Bastow, A. Ayele, M. Belachew, and G. W. Stuart (2012), Volcanism in the Afar Rift sustained by decompression melting with minimal plume influence, *Nat. Geosci.*, *5*, 406–409.
Shen, Y., S. C. Solomon, I. T. Bjarnason, and C. J. Wolfe (1998), Seismic evidence for a lower-mantle origin of the Iceland plume, *Nature*, *395*(6697), 62–65.
Simmons, N. A., A. M. Forte, and S. P. Grand (2007), Thermochemical structure and dynamics of the African superplume, *Geophys. Res. Lett.*, *34*, L02301, doi:10.1029/2006GL028009.
Smyth, J. R., D. J. Frost, F. Nestola, C. M. Holl, and G. Bromiley (2006), Olivine hydration in the deep upper mantle: Effects of temperature and silica activity, *Geophys. Res. Lett.*, *33*, L15301, doi:10.1029/2006GL026194.
Stixrude, L., and C. Lithgow-Bertelloni (2012), Geophysics of chemical heterogeneity in the mantle, *Annu. Rev. Earth Planet. Sci.*, *40*, 569–595.
Styles, E., D. R. Davies, and S. Goes (2011), Mapping spherical seismic into physical structure: biases from 3-d phase-transition and thermal boundary-layer heterogeneity, *Geophys. J. Int.*, *184*, 1371–1378, doi:10.1111/j.1365-246X.2010.04914.x.
Tackley, P. J. (2011), Living dead slabs in 3-D: The dynamics of compositionally-stratified slabs entering a "slab graveyard" above the core-mantle boundary, *Earth Planet. Sci. Lett.*, *188*, 150–162, doi:10.1016/j.pepi.2011.04.013.
Tauzin, B., E. Debayle, and G. Wittlinger (2008), The mantle transition zone as seen by global Pds phases: No clear evidence for a thin transition zone beneath hotspots, *J. Geophys. Res.*, *113*, B08309, doi:10.1029/2007JB005364.
Tauzin, B., E. Debayle, and G. Wittlinger (2010), Seismic evidence for a global low-velocity layer within the Earth's upper mantle, *Nat. Geosci.*, *3*, 718–721.
Tenner, T. J., M. M. Hirschmann, A. C. Withers, and P. Ardia (2012), H_2O storage capacity of olivine and low-Ca pyroxene from 10-13GPa: Consequences for dehydration melting above the transition zone, *Contrib. Mineral. Petrol.*, *163*, 297–316, doi:10.1007/s00410-011-0675-7.
Thompson, D. A., G. Helffrich, I. D. Bastow, J.-M. Kendall, J. Wookey, D. W. Eaton and D. B. Snyder (2011), Implications of a simple mantle transition zone beneath cratonic North America, *Earth Planet. Sci. Lett.*, *312*(1–2), 28–36, doi:10.1016/j.epsl.2011.09.037.
VanDecar, J. C., D. E. James, and M. Assumpcao (1995), Seismic evidence for a fossil mantle plume beneath South America and implications for plate driving forces, *Nature*, *378*(6552), 25–31.
Vinnik, L., and V. Farra (2007), Low S velocity atop the 410-km discontinuity and mantle plumes, *Earth Planet. Sci. Lett.*, *262*(3), 398–412.
Weidner, D. J., and Y. Wang (1998), Chemical- and Clapeyron-induced buoyancy at the 660 km discontinuity, *J. Geophys. Res.*, *103*(B4), 7431–7441.
Wilson, D., and R. Aster (2003), Imaging crust and upper mantle seismic structure in the southwestern United States using teleseismic receiver functions, *Leading Edge*, *22*(3), 232–237.
Wolfe, C. J., I. T. Bjarnason, J. C. VanDecar, and S. C. Solomon (1997), Seismic structure of the Iceland mantle plume, *Nature*, *385*(6613), 245–247.
Wolfe, C. J., S. C. Solomon, G. Laske, J. A. Collins, R. S. Detrick, J. A. Orcutt, D. Bercovici, and E. H. Hauri (2009), Mantle shear-wave velocity structure beneath the Hawaiian hot spot, *Science*, *326*(5958), 1388–1390.